ELSEVIER

Journal of Fluids and Structures 19 (2004) 49–62

JOURNAL OF FLUIDS AND STRUCTURES

www.elsevier.nl/locate/jnlabr/yjfls

A flow study around a time-dependent 3-D asymmetric constriction

J. Anagnostopoulos, D.S. Mathioulakis*

School of Mechanical Engineering/Fluids Section, National Technical University of Athens, 9 Heroon Polytechniou Ave., Zografos Athens 15710, Greece

Received 30 September 2002; accepted 13 October 2003

Abstract

The flow field around a time-dependent 3-D asymmetric tube constriction was studied and comparisons were made with the corresponding 2-D case. Both experimental (LDV-PIV) and numerical (finite volume) tools were employed for $\mathrm{Re}<1000$, $\mathrm{St}<0.3$ and 50% maximum passage reduction. The basic features of the flow were 3-D separation and reattachment, vortex generation especially after the middle of the cycle (max. constriction), and vortex destruction before the end of the cycle. The snake-type shape of the streamlines, known from the 2-D case, was not observed on the symmetry plane of the examined flow due to the secondary flow action.

1. Introduction

Flows in tubes of time-dependent cross-sectional area are met in many bioengineering applications. Blood flow in arteries is a characteristic example due to their moving walls and particularly in coronary arteries being squeezed during heart systole (Liu and Yamaguchi, 1999). The phenomenon of a self oscillating collapsible tube under small transmural pressure (Conrad, 1969; Kamm and Shapiro, 1979; Bertram et al., 1994; Kounanis and Mathioulakis, 1999), the operation of the so called "intra-aortic balloon pump" employed as a means for temporary heart assistance (Papaioannou et al., 2002) and the valveless pump (Manopoulos et al., 2001), are other physiological examples in which the flow is through tubes of time varying area either locally or along a certain length.

The flow field in a two dimensional (2-D) channel with a moving constriction has been studied in the past both numerically and experimentally by Pedley and Stephanoff (1985) and Ralph and Pedley (1988). The basic parameters involved in this problem are, the Reynolds number $\mathrm{Re}=U_bD/\nu$, where U_b is the mean bulk velocity, D the tube diameter and ν the kinematic viscosity, the Strouhal number $\mathrm{St}=fD/U_b$, where f is the frequency of the moving constriction, and finally the nondimensional amplitude of the constriction $\varepsilon=h/D$, where h is the amplitude of the constriction.

The basic element of the flow structure in a 2-D moving constriction for $\mathrm{Re}<1000$, $\mathrm{St}<0.1$ and $\varepsilon<0.5$ is the generation and propagation of a vortex train of alternate sign, close to the channel walls (Pedley and Stephanoff, 1985; Ralph and Pedley, 1988). The propagation speed of each vortex is inversely proportional to St, while its strength increases with Re. In the numerical study of Ralph and Pedley (1989) the flow field was examined using both viscous and inviscid momentum equations keeping the flow rate fixed either upstream or downstream of the constriction. Through this study it was found that even in case of zero viscosity, the flow field downstream of the constriction looked similar with the viscous one. However, there was a difference concerning vorticity, which did not decay in time for the

*Corresponding author. Tel.: +30-210-77-21-028; fax: +30-210-77-21-057.
E-mail address: mathew@fluid.mech.ntua.gr (D.S. Mathioulakis).

0889-9746/$ - see front matter © 2003 Elsevier Ltd. All rights reserved.
doi:10.1016/j.jfluidstructs.2003.10.002

inviscid case. Similar conclusions were drawn by Liu and Yamaguchi (1999), examining the case of a periodically compressed coronary artery using a 2-D approach. In the numerical work of Damodaran et al. (1999) in which the radius of a tube was locally time dependent, considering the flow axisymmetric it was found that vortices were generated close to the wall, imposing a waviness to the flow at the center of the tube.

Due to lack of evidence concerning the flow field around a three dimensional time-varying constriction, the present work was undertaken by employing both experimental and numerical tools.

2. Experimental procedure and techniques

A time-dependent constriction was established in a Plexiglas made square tube ($40 \times 40\,\text{mm}^2$) by a square piston of the same size, which moved periodically normal to the tube's axis (Fig. 1). In Fig. 1 the used Cartesian coordinate system (x, y, z) is shown, with $x = 0$ located at the downstream edge of the piston, $z = 0$ at the bottom of the tube and $y = 20\,\text{mm}$ on the plane of symmetry. The piston travelled a distance of 20 mm starting from a flush position and its period T was controlled by an adjustable speed DC motor. Water flow of a mean temperature of 20°C through the constriction was established by gravity, whereas the mean flow rate and its amplitude were adjusted by valves installed upstream and downstream of the constriction. The model was connected upstream to a settling chamber through a 2 m long square tube ($39.5 \times 39.5\,\text{mm}^2$) to suppress any flow disturbances and allow the flow reach the model at a fully developed state. In order to keep the downstream of the constriction flow rate fixed [this case was examined numerically for a 2-D flow field by Ralph and Pedley, 1989], the downstream valve was set at a relatively closed position, so that essentially the flow was fluctuating only upstream, measured by an electromagnetic flow meter (Fischer Porter).

The velocity field was measured by employing a one component Laser Doppler Velocimeter (LDV) as well as a 2-D Particle Image Velocimeter (PIV). The LDV system was used to measure the axial velocity component, which by phase averaging resulted in velocity profiles at various instants within a cycle of oscillation. LDV worked in the forward scatter mode incorporating a 15 mW He–Ne Laser, a bragg-cell for negative flow detection and a counter for signal analysis. The estimated dimensions of the measuring volume were 100 μm (width) by 600 μm (length). On the other hand, the PIV system, including a continuous light source (Argon Ion Laser, 300 mW) and a video recorder for storing flow images, provided velocity vectors on the symmetry plane. The velocity vectors at a given instant were calculated by cross correlating the odd and even fields of an image. The peak of the cross correlation function was designated by using a Gaussian scheme in both directions of the image plane, with a maximum error, based on artificial images, of 0.1 pixel. The interrogation windows were 32×64 pixels, with the longer direction in the streamwise one, and a 50% overlapping

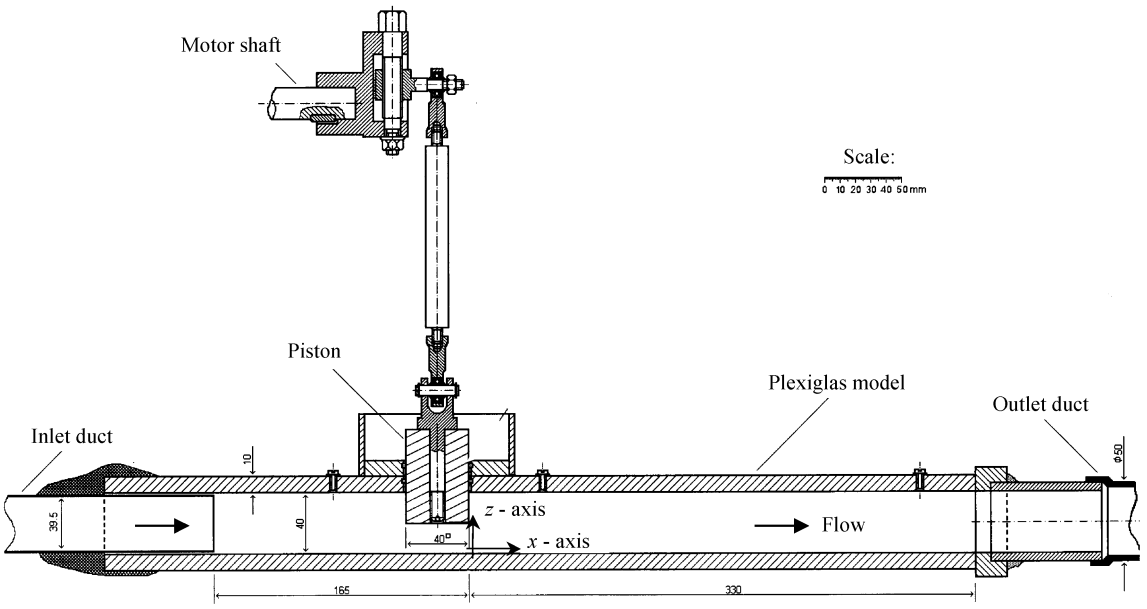

Fig. 1. Sketch of the model with the moving piston configuration. Dimensions are in mm.

was employed in both directions. According to the magnification factor, each interrogation window corresponded to an area of $2.5 \times 3.32\,\text{mm}^2$.

Due to the time consuming procedure of the LDV measurements, only one flow rate was examined, with a time mean value of 1.92 l/min (mean bulk velocity $U_b = 2\,\text{cm/s}$) and an oscillation period of 15 s. These corresponded to mean Re = 800, max Re = 968, min Re = 632, and St = 0.133. However, more combinations of Re and St were examined with PIV, namely mean Re varied in the range 300–800 and St between 0.05 and 0.3. For all the examined cases the downstream flow rate was kept constant.

3. Numerical solution methodology

The finite volume approach was used for the solution of the Navier–Stokes equations governing the time-dependent, incompressible, viscous flow:

$$\frac{\partial \boldsymbol{V}}{\partial t} + (\boldsymbol{V}\cdot\nabla)\boldsymbol{V} = \vec{g} - \frac{1}{\rho}\nabla p + \nu\nabla^2\boldsymbol{V}. \tag{1}$$

The equations are discretized on a Cartesian, collocated grid arrangement (Rhie and Chow, 1983), using a second order discretization scheme (Papadakis and Bergeles, 1995), whereas the solution is advanced in time with a fully implicit formula. For the 2-D and 3-D channel flows studied in this work, symmetric Poiseuille flow is set over the entire domain as initial condition, and the flow rate is fixed at either the channel inlet or outlet, depending on the corresponding experimental set-up. No-slip conditions are applied at all channel walls and at the indentation surfaces.

Unlike the works of Pedley and Stephanoff (1985) and Ralph and Pedley (1988), a fixed Cartesian mesh is used here, thus there is a need to simulate grid-cells partially or totally covered by the indentation. A 'partially blocked cells' Cartesian technique (Anagnostopoulos and Bergeles, 1999) is incorporated in the numerical code. As can be seen in Fig. 2(a) the grid cells are classified into four different types; A—internal cells (regular), B—boundary cells (free or partially blocked), C—overblocked (blocked above 50% but less than 100%), and D—solid cells (nonsolvable). In order to obtain 'fictitious' boundary values at the centers of the C-type cells (which are in the solid phase), the continuity equation is solved with a 'diffuse interface' approach, in which the exact interface is not considered. On the contrary, the location of the latter is taken into account when applying boundary conditions to the C-type cells (Fig. 2(a)), as in the 'sharp interface' methods. Geometric coefficients, γ_i, representing the free portion of the cell faces and volume are inserted in the equations for the B- and C-type cells, so the linearized governing Eq. (1), becomes:

$$\begin{aligned} &(A_P - \gamma_V S_P)\Phi_P = \sum_i \gamma_i A_i \Phi_i + \gamma_V S_U, \\ &A_P = \sum_i \gamma_i A_i, \quad i = E, W, N, S, U, D, \end{aligned} \tag{2}$$

where A_i are the coefficients linking the dependent variable Φ_P with its neighbors on the adjacent grid volumes, and S_U, S_P are additional source terms.

A key advantage of the above method is its ability to use the standard Cartesian stencils for the fluxes, derivatives etc. in all the cell types, regardless of the location and local orientation of the solid–fluid interface. The simplicity of the algorithm makes the method very efficient and easily applicable in either 2-D or 3-D complex geometries. Also, it preserves the accuracy of the boundary representation and retains the conservation property.

A second important advantage of the method appeared during its implementation in the present work: The necessary modifications to apply from a stationary to a moving boundary case are minor. The grid structure remains the same as

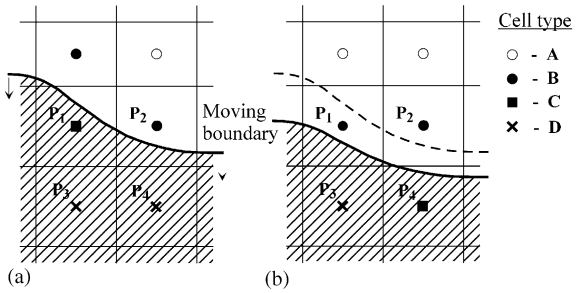

Fig. 2. Treatment of partially blocked cells, before (a), and after a boundary displacement (b).

the solid–fluid interface changes position and, unlike other 'sharp interface' methods, there is no need for grid reconstruction by cell-merging or cutting operations. Only the type and the geometric coefficients of some grid cells may change (Fig. 2), and the algorithm computes all changes automatically after each time-step.

Moreover, a special treatment for the 'freshly cleared' cells (e.g., Udaykumar et al., 2001), the 'solid' center of which emerges into the fluid at the next time-step, is not needed here. Fig. 2(a) shows for example that the overblocked cell P_1 is solved as such and keeps its own history in the fluid phase so that no discontinuity in time appears when it becomes B-type (Fig. 2(b)).

The system of discretized Eq. (2) is solved iteratively with the SIMPLE algorithm (Patankar and Spalding, 1972). Calculations in the next time-step start only after complete convergence in the previous step (implicit formula). In case of a repeated flow oscillation, a number of three to four complete cycles are calculated (starting form the Poiseuille flow solution) in order to obtain stabilized and fully periodic results throughout the channel.

4. Results and discussion

4.1. Validation of the numerical model

The computer code was at first validated on a 2-D problem, a channel with a moving indentation in one wall, for which detailed experimental and numerical results are available (Pedley and Stephanoff, 1985; Ralph and Pedley, 1988). The computational domain, sketched in Fig. 3, is covered with a uniform Cartesian grid of 802×62 nodes, which produces grid-independent results. Also, a small time-step size of $T/400$ secures the independency of the results. The displacement of the interface is given from the relation:

$$h(t) = \frac{h_{\max}}{2}\left[1 - \cos\left(2\pi \frac{t}{T}\right)\right]. \tag{3}$$

For the selected case [Case I, Ralph and Pedley (1988)], the wall movement amplitude $h_{\max}$ is 0.38 cm ($\varepsilon = 0.38$), whereas the resulting oscillation period T for the values $\mathrm{Re} = 507$ and $\mathrm{St} = 0.37$ equals 5.3308 s.

The resulting flow field at various instants is plotted in Fig. 4 and it is well compared to the corresponding numerical results of Ralph and Pedley (1988, Fig. 4). The propagation of the waves created due to the squeezing action of the constriction, results in the formation of a sequence of eddies with alternate sign at the top and the bottom of the channel. These eddies are marked with the letters A, B, C, D etc., according to the order of formation (Fig. 4). Their travelling speed is considerably lower than the propagation speed of the wave front. During the second half of the cycle, a secondary counter-rotating separation region is first formed in the eddy B (Fig. 4(b)), which grows and finally divides the eddy B into two co-rotating parts (Fig. 4(c)). The co-rotating part disappears quickly leaving kinked streamlines behind eddy B (Fig. 4(d)). Such streamlines can also be observed behind eddy C, but no duplication occurs there. During the last quarter of the cycle all eddies shrink quickly and swept downstream, leaving an almost undisturbed flow in the constriction region.

Numerical results for the position and phase speed of eddies B, C and D are compared with the corresponding measurements of Pedley and Stephanoff (1985) in Fig. 5. The crests and troughs of the eddies are represented by the points of maximum and minimum displacement of the core streamlines. The dotted lines correspond to the crests and troughs of the secondary vortices formed in the vicinity of eddies B and C. The agreement is quite satisfactory, verifying that the present simulation can successfully reproduce the unsteady viscous effects in such flows.

4.2. The 3-D constriction

The flow in a square tube with a time-dependent constriction (Fig. 1) was studied both experimentally and numerically under the following conditions: mean $\mathrm{Re} = 800$, max $\mathrm{Re} = 968$, min $\mathrm{Re} = 632$, $\mathrm{St} = 0.133$ ($T = 15$ s), and maximum constriction amplitude $h_{\max} = D/2$, where D is the side of the square tube. The computational domain was $12.5D$ (0.5 m) in length and covered the entire tube width, in order to be able to identify any nonsymmetric behavior of the flow. Several numerical grids of increasing density, as well as various time-steps were tested to check the dependency of the results on the discretization intervals. The combination of a $202 \times 43 \times 43$ nodes uniform grid with a time-step of $T/300$ was found to reproduce the flow behavior with satisfactory accuracy, although the results are not fully independent. As can be seen in Figs. 6 and 8, the results with this mesh and with a coarser one, having $152 \times 33 \times 33$ nodes, are identical upstream of the piston but considerable differences may appear in some very unstable regions and at certain time instants, as below the piston (Fig. 6(b)), or far downstream (Fig. 8). More elaborate results could be

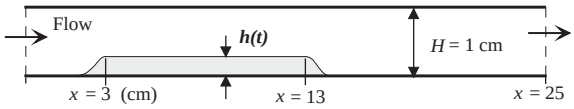

Fig. 3. Computational domain used to simulate the test case of Ralph and Pedley (1988).

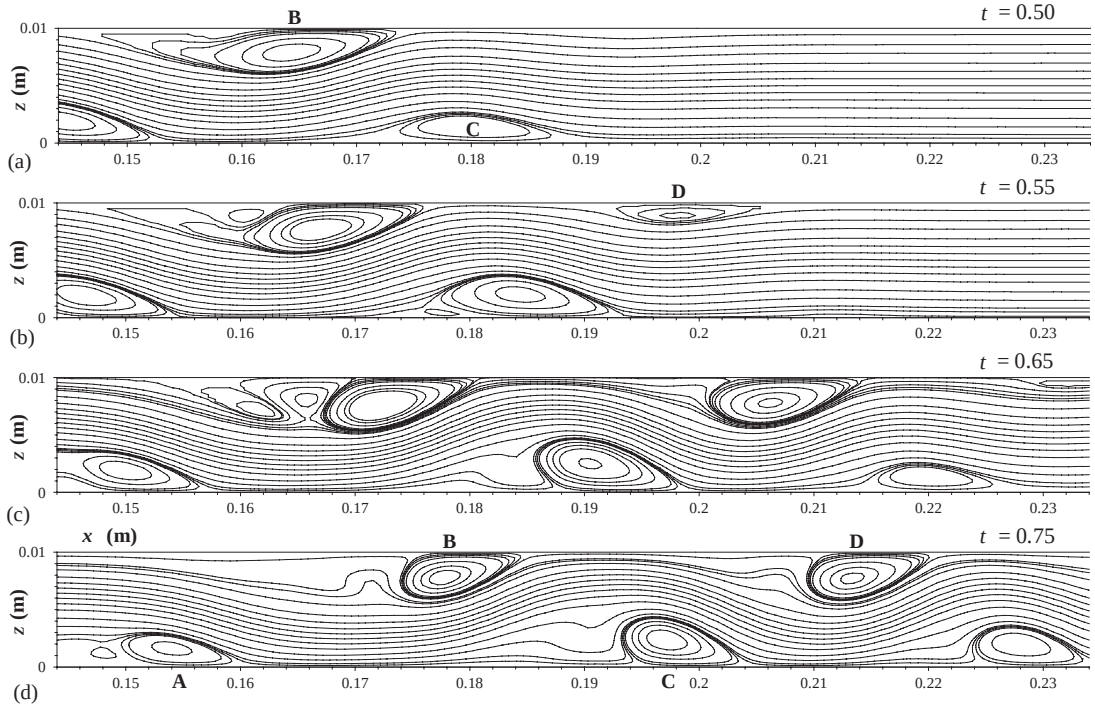

Fig. 4. Calculated flow streamlines at various time instants (nondimensional) for the 2-D channel of Ralph and Pedley (1988) with flow conditions: Re = 507, St = 0.37, $\varepsilon = 0.38$.

obtained there using even finer meshes or other numerical techniques (e.g., local grid refinement), but with much more computer cost. However, the present accuracy was considered adequate for the scope of this work.

The flow behavior around the time varying constriction is shown in Figs. 6 and 8 through various characteristic axial velocity time-records obtained by LDV and the numerical method. Time $t = 0$ in the above figures corresponds to the flush position of the piston. Upstream of the constriction the flow rate changes harmonically in time, being reduced when the piston enters the tube. Based on the continuity equation and the fact that the downstream flow rate is fixed, the upstream flow rate is a function of the piston velocity. Namely, at $t = T/4$ the flow rate takes its minimum value, since the piston enters the tube with its highest velocity. The opposite happens at $t = 3T/4$ at which flow peak occurs because the piston retraction velocity maximizes. A typical time-record of the axial velocity is shown in Fig. 6(a) at the center of the tube, 40 mm upstream of the piston, exhibiting an oscillatory variation. However, the time instant at which a velocity minimum occurs changes from point to point, as well as its amplitude. Specifically the velocity amplitude is higher close to the tube walls (where the mean velocity is low) compared with that at the center, a phenomenon which is characteristic of pulsating flows in tubes (Richardson and Tyler, 1929). A similar behavior has been documented in external flows exposed to oscillating free streams, in which both the velocity amplitude and phase angle change across the boundary layer (Mathioulakis and Telionis, 1987).

Fig. 6(b) and (c) refer to the region below the piston, presenting time records on the symmetry plane ($y = 20$ mm) as well as close to the tube sidewall ($y = 4$ mm), 2 mm below the tube axis ($z = 18$ mm). The flow in this region is in phase with the motion of the piston, being increased when the piston enters the tube (when the flow passage is reduced). However, close to the bottom piston wall the flow separates at the symmetry plane after the piston reaches its final position inside the tube. As a result, the axial velocity time record drops from a positive peak value to negative ones, in the middle of the period (LDV data of Fig. 6(b)). On the same z plane the flow is always attached close to the sidewalls

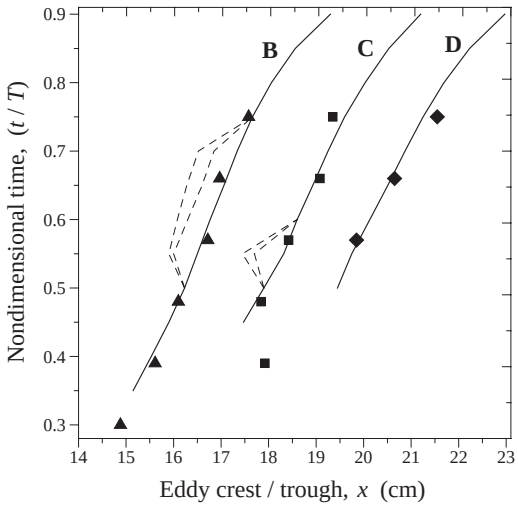

Fig. 5. Comparison between computed and measured position and speed of eddies B, C, and D. Solid lines—predictions; symbols—experiments (Pedley and Stephanoff, 1985); dotted lines—secondary eddies (see also Fig. 4).

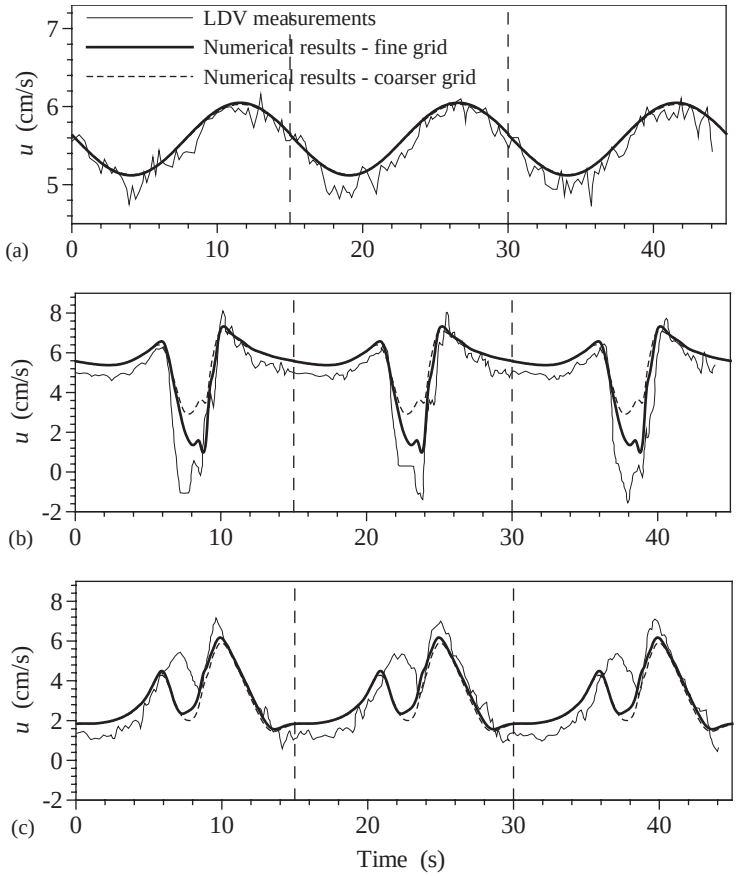

Fig. 6. Computed and measured by LDV velocity time records in the square tube: (a) upstream of the constriction, at $(x, y, z) = (-80, 20, 20\,\text{mm})$; (b) below piston, at (–20, 20, 18 mm); (c) below piston, at (–20, 4, 18 mm).

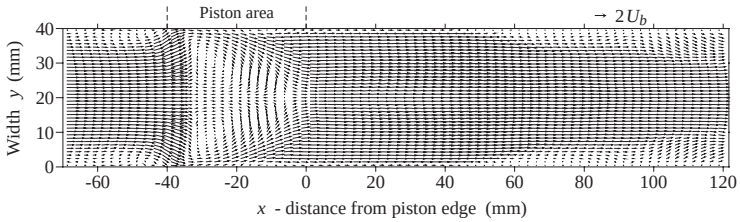

Fig. 7. Predicted velocity vectors at the horizontal plane $z = 20$ mm, $t = 9T/15$.

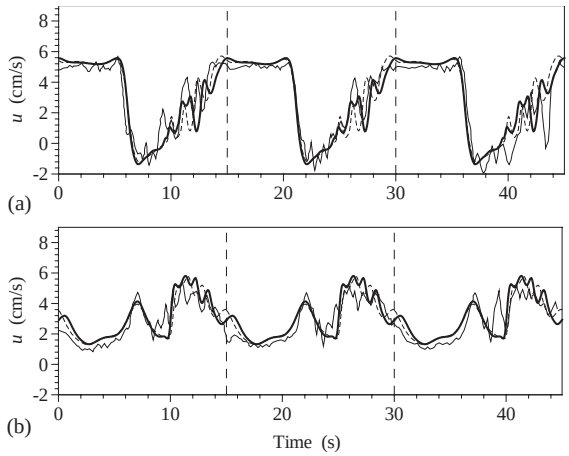

Fig. 8. Computed and measured by LDV velocity time records in the square tube downstream of the constriction, at $x = 30$ mm, $z = 24$ mm and: (a) $y = 20$ mm (symmetry plane); (b) $y = 4$ mm (near tube sidewall). Legend as in Fig. 6.

(Fig. 6(c)) showing the three dimensional character of the flow. Negative velocities are not shown in the numerical predictions of Fig. 6(b) but they do appear 2 mm above this, at $z = 20$ mm (Fig. 7). In other words, this recirculation region was underpredicted, most probably due to the grid resolution, which close to the bottom piston side seems to be not fine enough to reproduce exactly the steep velocity gradient there. However, the three-dimensionality of the flow under the piston is illustrated clearly in Fig. 7, in which the velocity vectors under the piston at $z = 20$ mm and $t = 9T/15$ are positive and greater close to the tube sidewalls compared to the small, negative values on the symmetry plane.

Downstream of the piston and when this enters the tube, a recirculation zone is formed, which is associated with discrete vortex formation and strong three-dimensionality, especially when the piston retracts to its initial position at the second half of the cycle. The propagation of the vortices, which are formed at the shear layer in the extension of the piston bottom wall, as well as at the separated region under the piston itself (see below for more details), are recognized as disturbances in the velocity time records. Such disturbances can be observed in both the measured and calculated time records of Fig. 8, with a fairly good agreement.

Phase-averaged streamwise velocity profiles on the symmetry plane ($y = 20$ mm), and on a plane normal to this at $z = 18$ mm are shown in Fig. 9(a) and (b), at $t = T/2$. The agreement between predictions and experiment seems to be good in general. Discrepancies are more evident downstream of the piston in Fig. 9(a), where the flow is very unstable, and most probably the five measuring cycles, which were used to extract the phase-averaged velocity profiles, are not enough. Also, the discrepancies just below the piston (Fig. 9(b)) can be attributed to the relatively coarse numerical grid there, as stated previously. A proof of this is that the predicted velocity profiles of Fig. 7 ($z = 20$ mm) are similar to the measured of Fig. 9(b) ($z = 18$ mm).

By employing PIV on the symmetry plane it was possible to detect details of the flow field which could not be recognized by LDV, obtaining a more global picture of the flow. When the piston enters the tube, an anticlockwise vortex is generated between the piston upstream side and the top tube wall (Fig. 10(a)). The size of this vortex increases while the piston proceeds to its final position and it shrinks, when its motion direction reverses. At the same time a stagnation point appears close to the moving piston, being nonstationary since it translates parallel to the moving wall. At the piston upstream corner the flow accelerates and turns towards the bottom tube wall. This change of the flow

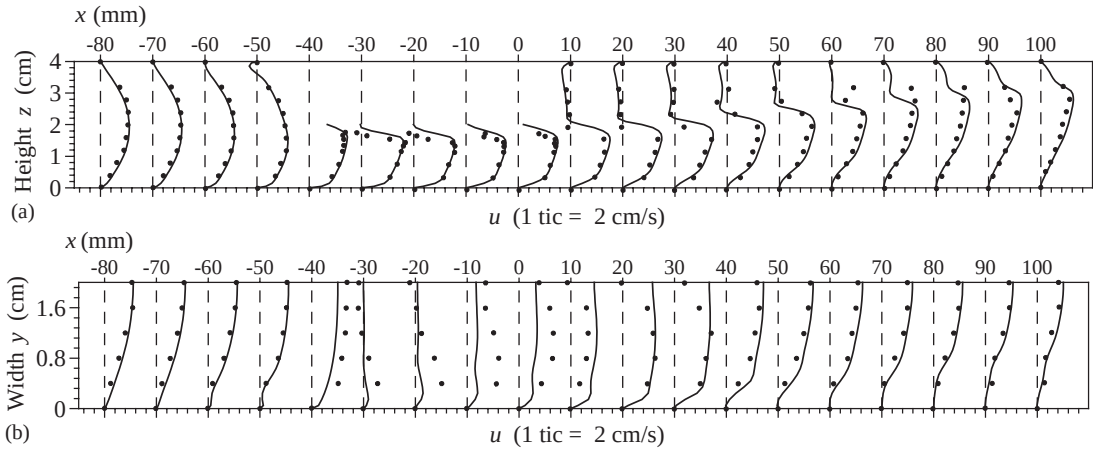

Fig. 9. Comparison between calculated and LDV-measured velocity profiles in the square tube, at $t = T/2$: (a) on the symmetry plane, $y = 20$ mm, and (b) on a horizontal plane $z = 18$ mm.

direction also takes place in a region upstream of the piston, the size of which depends not only on time but also on Re and St. More specifically, it was observed that for a mean Re = 480 and St = 0.05 this region increases and decreases in phase with the moving piston. However, keeping Re constant and increasing St to 0.1, a phase lag was observed so that when the piston retracts, the flow disturbances keep on travelling upstream.

The flow is attached under the piston till $t = T/2$, when a separation bubble begins to form. When the piston starts moving back to its flush position, an adverse pressure gradient develops due to the passage area increase, resulting in the formation of a shear layer, emanating from the upstream corner of the piston. This shear layer rolls-up into discrete vortices (Fig. 10(b)), which grow as time proceeds, being shed finally into the flow field. At the same time the shear layer, which is formed in the extension of the piston's lower side, rolls-up into discrete vortices as well (Fig. 10(c)). All these vortices propagate downstream and induce disturbances to the flow, which as mentioned previously are detected in the velocity time records in the second half of the cycle ($T/2 < t < T$), (Fig. 8). The characteristic roll-up of the free shear layer emanating from the downstream corner of the piston is also shown in Fig. 11, based on flow visualization a few instants after the piston had reached its lowest position. A similar behavior was predicted by the numerical method (Fig. 12) at $t = 2T/3$ on the symmetry plane. Downstream of the piston the flow separates at the top tube wall, a characteristic picture of which on the symmetry plane is shown in Fig. 10(d), with a well shaped vortex at a time instant before the piston has reached its lowest position. However, the coherence of this vortex does not last long, so that it is completely destroyed before the piston returns to its flush position.

In order to compare the velocity fields produced by a moving indentation in a 2-D channel with that of the present 3-D model, the numerical method was applied to a 2-D channel having common dimensions (size of piston, distance between top and bottom walls) with those of Fig. 1. The flow conditions (Re, St, h_{max}) were also kept the same, as well as the grid density along the x and z directions. The predicted velocity fields in both channels are presented in Fig. 13, at $t = T/2$. The basic difference between these flow fields is that for the 3-D case there is no vortex formed on the symmetry plane, so that the snake-type shape of the streamlines known from the 2-D case does not appear.

In order to shed more light into this complex 3-D flow field, axial velocity contours and secondary flow velocity vectors were drawn at various instants and cross-sections, based on the results of the numerical method. Flow separation downstream of the piston resembles the flow field in curved tubes (Berger et al., 1983; Humphrey et al., 1985) and tube bifurcations (Hofer et al., 1996; Schinas and Mathioulakis, 2000). Hence, axial flow reversal is met at the top tube wall as well as around the axis of symmetry, on which negative velocities appear up to the tube center (Fig. 14(a)–(c)). At the same time, two counter rotating vortices of the secondary flow are established at the upper half of the cross-section, above the detached (from the piston) shear layer, pushing the fluid in a direction from bottom to top along the sidewalls. These vortices influence the axial velocity component in a sense that this progressively increases not at the symmetry plane but close to the sidewalls. Therefore, regions of almost stagnant fluid close to the piston back face gain considerable momentum in a small streamwise distance, while at the symmetry plane the flow does not change significantly. Focusing on the symmetry plane (Fig. 13(b)) we notice that the line which divides the reversed flow from the positive one is almost straight, in contrast to the 2-D case (Fig. 13(a)) in which this line is curved towards the reattachment point. Only close to the sidewalls ($y = 5$ mm) the 3-D flow picture resembles the 2-D case with regard to two almost stationary recirculating regions, formed one at the top tube wall next to the piston and the other at the

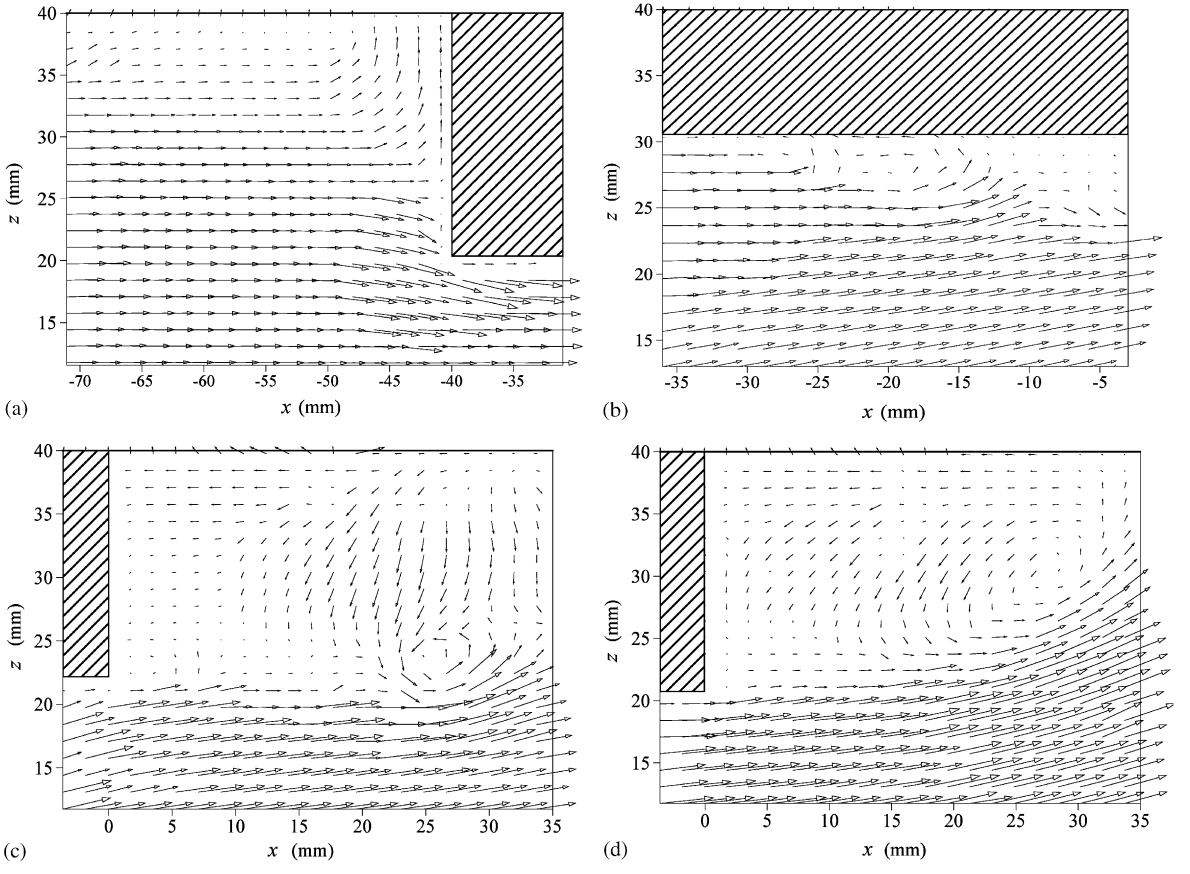

Fig. 10. Velocity vectors on the symmetry plane of the square tube, obtained by the PIV system: (a) upstream of the piston, $t/T = 0.5$; (b) under the piston, $t/T = 0.76$; (c) downstream of the piston, $t/T = 0.61$; (d) downstream of the piston, $t/T = 0.43$.

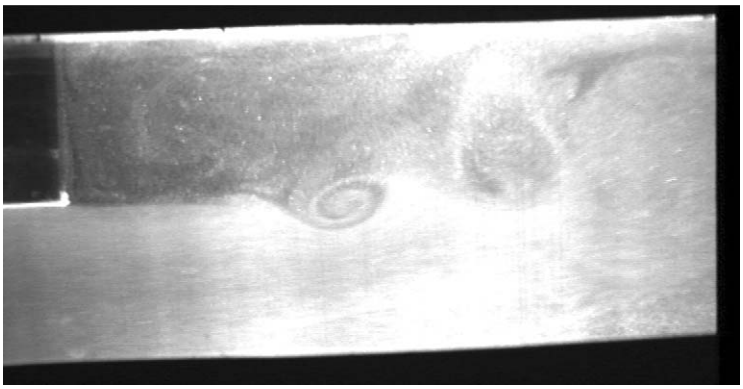

Fig. 11. Video image of the flow field downstream of the piston, $t/T = 0.6$.

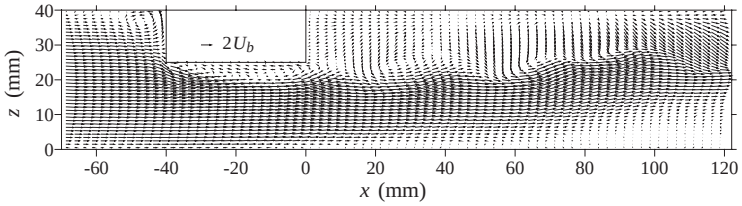

Fig. 12. Predicted velocity vectors on the symmetry plane ($y = 20$ mm), at $t = 2T/3$.

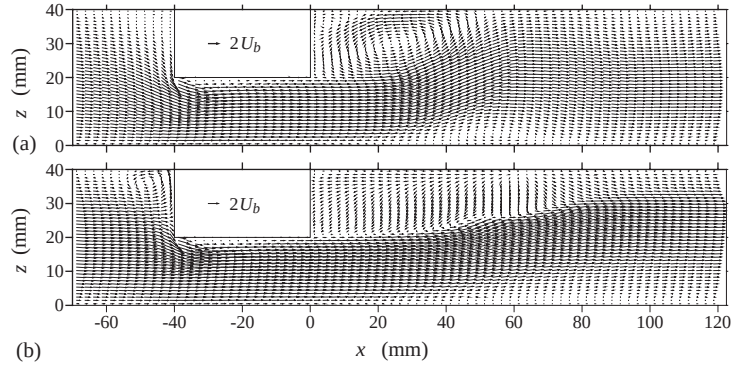

Fig. 13. Comparative view of the flow patterns computed at $t = T/2$ for the same flow conditions, in: (a) 2-D and (b) square tube—symmetry plane.

bottom (Fig. 15). It is reminded that in the 2-D case there are not only two but many more vortices (Fig. 4) along the two walls, moving downstream.

Although there are similarities between the examined flow and the flow in curved tubes and tube bifurcations (e.g., curved streamlines, secondary flow vortices, similar shapes of axial velocity contours), it should be emphasized that there is a major difference here: the velocity along the curved streamlines below the piston is maximum close to it (Fig. 13(b)), namely close to the streamlines center of curvature. On the other hand, it is well documented that in a curved tube, a parabolic velocity profile is converted to a skewed one with its maximum far from the center of curvature (Berger et al., 1983). It should be also noted that in the present flow the number of secondary vortices does not remain the same in all cross-sections, thus making the flow picture look even more complex. For instance, in Fig. 14(a), besides the vortex pair at the upper half of the cross-section, there are two more weak vortex pairs close to the sidewalls of the lower half cross-section. However, the latter vortices decay in the next downstream stations (Fig. 14(b) and (c)), while at $x = 56.3$ mm (Fig. 14(d)) another vortex pair is formed close to the top wall, counter rotating with respect to that close to the axis of symmetry. This new vortex pair appears downstream of the two nodal points of reattachment (see below). Normally one or two vortex pairs were present in all the cross-sections and for all time instants. In curved tubes of

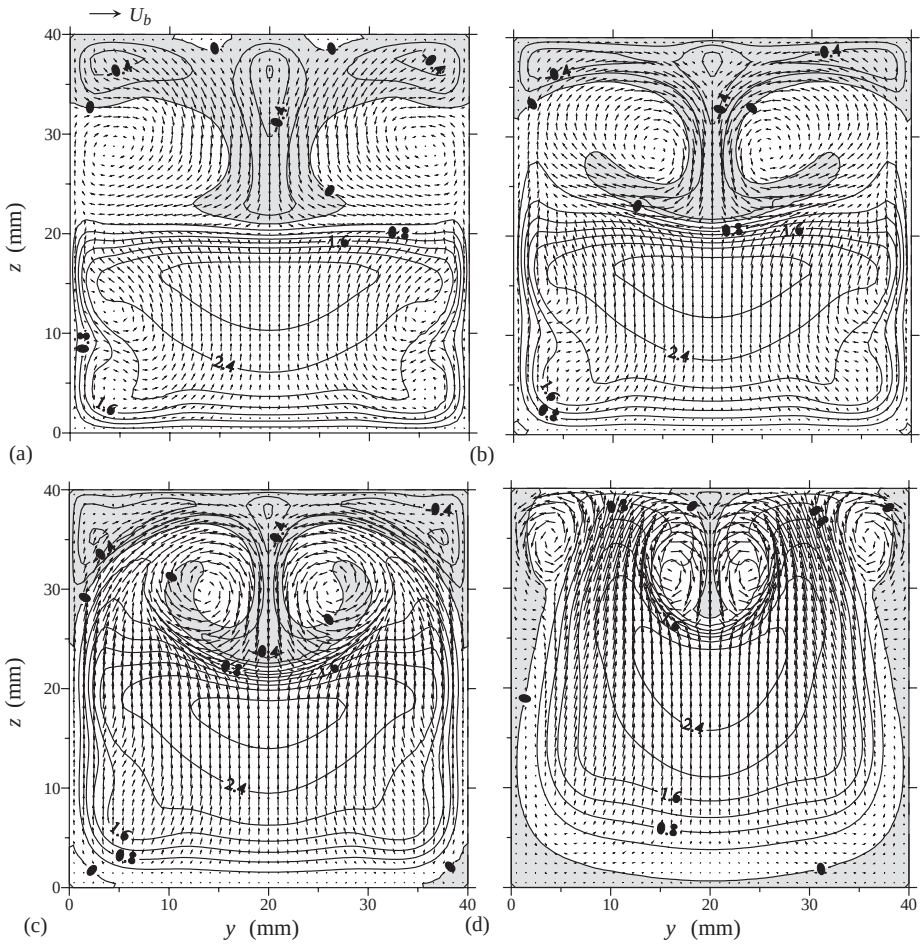

Fig. 14. Predicted velocity field at various tube cross-sections ($t = T/2$): (a) $x = 6.25$ mm, (b) $x = 18.75$ mm, (c) $x = 31.25$ mm, (d) $x = 50.25$ mm. Contour lines refer to nondimensionalized by U_b axial velocity, and vectors represent secondary flow velocities.

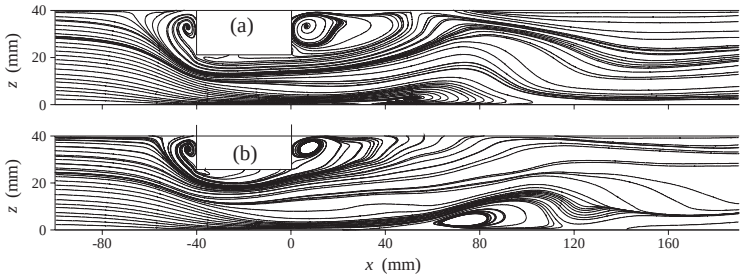

Fig. 15. Computed limiting streamlines on plane $y = 5$ mm at (a) $t = T/2$ and (b) $t = 2T/3$.

rectangular cross-section a numerical analysis by Winter (1987) showed (varying the axial pressure gradient, the aspect ratio of the cross-section and the tube curvature) that the flow solution goes from one to two vortex pairs. Moreover, for unsteady flow in a curved tube, Chang and Tarbell (1985) predicted seven vortex pairs in a cross-section at a given time instant. Also, in a 90° square tube bifurcation under pulsating flow conditions, it was found (Nikolaidis and Mathioulakis, 2002) that the number of secondary flow vortices at a cross-section was a function of time. Another common feature between the examined flow and the flow in curved square tubes is the negative flow at the corners between the outer wall and the sidewalls (Chung and Hyun, 1992) attributed to the adverse pressure gradient associated

with the curved streamlines. Fig. 14(b) and (c) include such negative flow regions at the lower corners of the tube, which further downstream expand along both the bottom and sidewalls (Fig. 14(d)).

Examining the flow close to the solid surfaces of the model at a distance of 1 mm, interesting flow features were revealed (Fig. 16). At $t = T/2$ (Fig. 16(a)) there is a separation bubble under the piston, covering a part of its surface. Close to the sidewalls the flow is attached, so that the axial velocity profile looks like that obtained by LDV (Fig. 9(b)). The reversed flow downstream of the piston extends up to about $x = 50$ mm at this instant, where two stagnation points appear on the top tube wall, resembling the nodal points of attachment, as described by Tobak and Peake (1982) in their topological study of three dimensional flows. The flow around each of these points looks like the flow of a source from which streamlines emanate, which however, in this case are not straight. These lines converge along the symmetry plane, on which the change of the velocity sign from negative to positive occurs downstream of the two singular points. For a certain distance downstream of these points the flow turns both towards the plane of symmetry and the sidewalls. This is the region where two counter-rotating vortex pairs exist in the upper half of the cross-section, as mentioned before (Fig. 14(d)). At $t = 2T/3$ (Fig. 16(b)), the reversed flow region at the top tube wall has expanded further downstream (although the constriction is smaller than in Fig. 16(a)), and negative velocities under the piston cover its whole length about the plane of symmetry. The furthest distance from the piston at which negative velocities were found on the top tube wall, for all the examined instants, was about 90 mm. On the bottom wall of the tube (Fig. 16(c)), the velocity vectors are in general very small, besides an area opposite to the piston where the flow is forced to pass through the constriction, showing two maxima off center.

Based on the velocity vectors close to the top tube wall (1 mm far), the axial wall shear rate along the symmetry plane (wsr) was examined, in analogy to the wsr in the inner side of a curved tube. In the latter case it has been found that in the entrance of a curved tube, wsr goes through a minimum without changing sign (Talbot and Wong, 1982; Stewartson

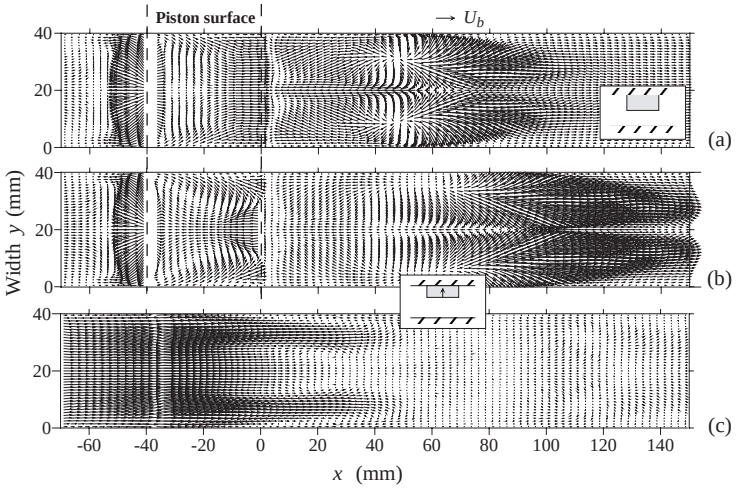

Fig. 16. Predicted velocity vectors at a distance of 1 mm from the tube walls: (a) top wall, $t = T/2$; (b) top wall, $t = 2T/3$; (c) bottom wall, $t = 2T/3$. The area between the dotted lines is under the bottom face of the piston.

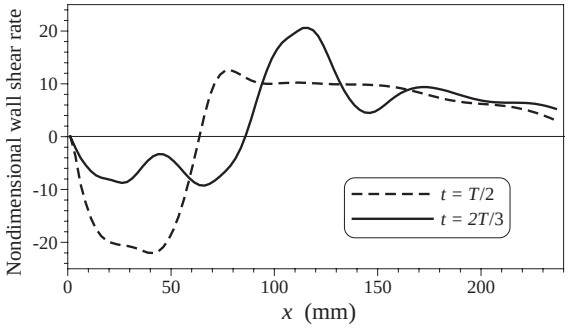

Fig. 17. Axial wall shear rate along the symmetry line on top tube wall, $t = T/2$ and $t = 2T/3$. Nondimensionalized by U_b and D.

and Simpson, 1982), being attributed to the so called boundary layer collision of the secondary flow, which forces the axial flow far from the surface, reducing wsr. In our case (Fig. 17(a) and (b)) there was no such an indication. Here, wsr becomes negative just after the piston, as expected due to the recirculation flow zone, it goes through a minimum and then it changes sign. Comparing the two curves of Fig. 17 we notice that at $t = 2T/3$ the curve is more wavy compared to $t = T/2$, due to the shed vortices which are introduced into the flow field at $t > T/2$. The flow becomes quite unstable after $t = T/2$, when the separation bubble under the piston bursts (Fig. 12). In the beginning of the next cycle, flow instabilities are pronounced far from the piston, since any disturbances of the previous cycle travel downstream. However, despite the significant flow instabilities, no asymmetries were found with respect to the plane of symmetry.

5. Conclusions

The flow field in a time-dependent 3-D asymmetric tube constriction (moving piston in a square tube) was studied both experimentally and numerically, providing comparisons with the corresponding 2-D case. The cross-sectional area at the constriction was changing periodically in time between 0 and one half of the tube cross-section, Re was below 1000, St smaller than 0.3, and the downstream flow rate was kept fixed.

The main feature of this unsteady flow field was vortex formation especially during the retracting phase of the piston below and downstream of it, due to flow separation. Many similarities were found with the flow in curved tubes and tube bifurcations concerning streamline curvature, axial flow velocity contours shapes, and secondary flow vortex pairs downstream of the constriction. Due to the existence of secondary flow vortices the flow picture on the symmetry plane did not have much in common with the corresponding 2-D case. Only close to the side tube walls the two flow fields looked somehow similar, concerning the two vortices (one next to the piston and another at the opposite bottom wall), which however were almost stationary in the 3-D channel, whereas in the 2-D case there were more vortices moving downstream. In general, differences between 2-D and 3-D case seem to be extensive, so that someone has to be very cautious before transferring any conclusions from the one case to the other.

Interesting flow features of the 3-D case were also the flow separation and reattachment at the top tube wall where two stagnation points appear, the 3-D separation zone under the piston, the shear layer roll-up both under the piston and downstream of it and finally, the secondary flow vortex pairs, the number of which changes streamwise.

Comparisons between experimental (LDV-PIV) and numerical results were in general good. Discrepancies were more evident downstream of the piston, where the flow was highly disturbed, especially when the piston returned to its initial flush position, as well as close to the bottom wall of the piston, where velocity gradients were very steep.

Acknowledgements

The authors are grateful to Messrs Joseph and Thomas Davides for their excellent job on making the moving constriction model, as well as to the valuable criticism of the reviewers.

References

Anagnostopoulos, J., Bergeles, G., 1999. 3-Dimensional modeling of the flow and the interface surface in a continuous casting mold model. Metallurgical and Materials Transactions B 30B, 1095–1105.

Berger, S.A., Talbot, L., Yao, L.-S., 1983. Flow in curved pipes. Annual Review of Fluid Mechanics 15, 461–512.

Bertram, C.D., Sheppeard, M.D., Jensen, O.E., 1994. Prediction and measurement of the area-distance profile of collapsed tubes during self-excited oscillations. Journal of Fluids and Structures 8, 637–660.

Chang, L.-J., Tarbell, J.M., 1985. Numerical simulation of fully developed sinusoidal and pulsatile (physiological) flow in curved tubes. Journal of Fluid Mechanics 161, 175–198.

Chung, J.H., Hyun, J.M., 1992. Convective heat transfer in the developing flow region of a square duct with strong curvature. International Journal of Heat and Mass Transfer 35 (10), 2537–2550.

Conrad, W.A., 1969. Pressure-flow relationships in collapsible tubes. IEEE Transactions on Biomedical Engineering BME-16, 284–295.

Damodaran, V., Rankin, G.W., Zhang, C., 1999. Effect of a moving boundary on pulsatile flow of incompressible fluid in a tube. Computational Mechanics 23, 20–32.

Hofer, M., Rappitsch, G., Perktold, K., Trubel, W., Schima, H., 1996. Numerical study of wall mechanics and fluid dynamics in end-to-side anastomoses and correlation to intimal hyperplasia. Journal of Biomechanics 29 (10), 1297–1308.

Humphrey, J.A.C., Iacovides, H., Launder, B.E., 1985. Some numerical experiments on developing laminar flow in circular-sectioned bends. Journal of Fluid Mechanics 154, 357–375.

Kamm, R.D., Shapiro, A.H., 1979. Unsteady flow in a collapsible tube subjected to external pressure or body forces. Journal of Fluid Mechanics 95, 1–78.

Kounanis, K., Mathioulakis, D.S., 1999. Experimental flow study within a self oscillating collapsible tube. Journal of Fluids and Structures 13, 61–73 doi:10.1006/jfls.1998.0194.

Liu, H., Yamaguchi, T., 1999. Computer modeling of fluid dynamics related to a myocardial bridge in a coronary artery. Biorheology 36, 373–390.

Manopoulos, Ch.G., Pappou, Th., Mathioulakis, D.S., Tsangaris, S., 2001. Theoretical models and experimental study of valveless pumping in the circulatory system. In: Muller, R., Gerber, H., Stacoff, A. (Eds.), International Society of Biomechanics XVIIIth Congress, Book of Abstracts. Interrepro AG, Zurich, pp. 335.

Mathioulakis, D.S., Telionis, D.P., 1987. Velocity and vorticity distributions in periodic separating laminar flow. Journal of Fluid Mechanics 184, 303–333.

Nikolaidis, N.M., Mathioulakis, D.S., 2002. Axial and secondary flow study in a 90 deg bifurcation under pulsating conditions using PIV. Journal of Fluids Engineering 124, 505–511 doi:10.1115/1.1470478.

Papadakis, G., Bergeles, G., 1995. A locally modified second order upwind scheme for convection terms discretization. International Journal for Numerical Methods in Heat and Fluid Flow 5, 49–62.

Papaioannou, T.G., Mathioulakis, D.S., Nanas, J.N., Tsangaris, S.G., Stamatelopoulos, S.F., Moulopoulos, S.D., 2002. Arterial compliance is a main variable determining the effectiveness of intra-aortic balloon counterpulsation: quantitative data from an in vitro study. Medical Engineering and Physics 24, 279–284.

Patankar, S.V., Spalding, D.B., 1972. A calculation procedure for heat, mass and momentum transfer in 3-dimensional parabolic flows. International Journal of Heat and Mass Transfer 15, 1787–1806.

Pedley, T.J., Stephanoff, K.D., 1985. Flow along a channel with a time-dependent indentation in one wall: the generation of vorticity waves. Journal of Fluid Mechanics 160, 337–367.

Ralph, M.E., Pedley, T.J., 1988. Flow in a channel with a moving indentation. Journal of Fluid Mechanics 190, 87–112.

Ralph, M.E., Pedley, T.J., 1989. Viscous and inviscid flows in a channel with a moving indentation. Journal of Fluid Mechanics 209, 543–566.

Rhie, C.M., Chow, W.L., 1983. Numerical study of a turbulent flow past an airfoil with trailing edge separation. AIAA Journal 21, 1525–1532.

Richardson, E.G., Tyler, E., 1929. The transverse velocity gradient near the mouths of pipes in which an alternating or continuous flow of air is established. The Proceedings of the Physical Society 42/1 (231), 1–15.

Schinas, D., Mathioulakis, D.S., 2000. Pulsating flow in a 90 degree bifurcation. Journal of Fluids Engineering 122, 569–575 doi:10.1006/jcph.2001.6916.

Stewartson, K., Simpson, C.J., 1982. On a singularity initiating a boundary-layer collision. Quarterly Journal of Mechanics and Applied Mathematics 35, 1–16.

Talbot, L., Wong, S.J., 1982. A note on boundary-layer collision in a curved pipe. Journal of Fluid Mechanics 122, 505–510.

Tobak, M., Peake, D., 1982. Topology of three-dimensional separated flows. Annual Review of Fluid Mechanics 14, 61–85.

Udaykumar, H.S., Mittal, R., Rampunggoon, P., Khanna, A., 2001. A sharp interface Cartesian grid method for simulating flows with complex moving boundaries. Journal of Computational Physics 174, 345–380 doi:10.1006/jcph.2001.6916.

Winter, K.H., 1987. A bifurcation study of laminar flow in a curved tube of rectangular cross-section. Journal of Fluid Mechanics 180, 343–369.